2014 Canada-China Conference on Advanced Reactor Development (CCCARD-2014)
Niagara Falls Marriott Fallsview Hotel & Spa, Niagara Falls, Ontario Canada, April 27-30, 2014.

CCCARD2014-043

NUMERICAL STATIC INSTABILITY ANALYSIS OF SUPERCRITICAL WATER FLOWING UPWARD IN A VERTICAL CHANNEL

E. Ebrahimnia[1], V. Chatoorgoon[1], S. Ormiston[1] and L. Leung[2]
[1] University of Manitoba, Manitoba, Canada
[2] Atomic Energy of Canada Limited, Chalk River, Ontario, Canada

Abstract

Numerical stability analysis of supercritical water flowing upward in a vertical heated pipe is carried out using a RANS model in the CFD ANSYS CFX v14.5 code. Threshold of static instability is determined using the *k*-*ε* and the SST turbulence models. Results are compared with 1-D non-linear code solutions. Also, existing conditions for approximating the static instability threshold are assessed. Results show relatively good agreement between the instability results of the *k*-*ε* and the SST turbulence models. Also, results show that approximating the flow instability threshold by existing conditions based on steady-state results hold true for a CFD solution.

Introduction

The Supercritical Water Reactor (SCWR) has been proposed by the U.S. DOE Nuclear Energy Research Advisory Committee and the Generation IV International Forum [1] as one of the six designs for new Generation IV reactors. SCWRs are one of the three types of Light Water Reactors (LWRs). The other types are Boiling Water Reactors (BWRs) and Pressurized Water Reactors (PWRs). Using supercritical water in reactors as a primary coolant is believed to provide an improvement in overall plant efficiency compared to other types of LWRs (~45% versus ~33% of other LWRs). Considerable design simplification is another feature of a SCWR, which distinguishes it from a BWR and a PWR. However, despite the benefits of supercritical water in terms of overall efficiency, thermal hydraulic instabilities are likely to arise in supercritical water reactors due to the sharp variations of some physical properties (mainly the density) along a heated pipe. A flow is stable if, when disturbed, its new operating conditions tend asymptotically towards the original initial condition; otherwise, the flow is said to be unstable. Two different kinds of instabilities have been encountered: static (also called excursive), and dynamic (also called oscillatory and density-wave oscillation). Static instability, which is the focus of this study, happens when following a disturbance, the flow moves away from its equilibrium position in an excursive manner without returning to the original state. Static instability is dangerous as the flow rate might go to zero and lead to burnout of the channel. It is an undesirable phenomenon and flow conditions should be designed with a sufficient margin against it to assure the safety of SCWRs.

A significant number of analytical and numerical analyses on the stability of supercritical flows have been reported in recent years. Bouré et al. [2] presented a classification of different types of instabilities. They suggested that a static instability (Ledinegg instability) can be described using

only the steady-state equations. In this case, a small change in the flow conditions results in a new steady-state not equal to the original one. For dynamic instabilities, such as density-wave oscillations, the steady-state equations are not sufficient to predict the system behavior or the threshold of instability. Chatoorgoon [3] performed a study to develop non-dimensional parameters for predicting the static instability boundary, using an in-house linear instability code. He concluded that static instability is most likely to happen in vertical down-flow and least likely to occur in vertical up-flow, while oscillatory instability can occur at higher temperatures in down-flow.

In recent years, there has been an increase in use of CFD (Computational Fluid Dynamics) simulations in stability analysis of supercritical flow. Ampomah-Amoako and Ambrosini [4] studied the performance of CFD in analyzing the supercritical flow stability. They used the STAR-CCM+ code and compared the CFD instability threshold results with the results of their in-house 1-D code [5] for a circular pipe, as well as a triangular and a square pitch rod bundle slices. Their work confirmed the occurrence of both static and dynamic instabilities depending on the inlet fluid sub-cooling. To find the instability boundary, they first chose an inlet mass flow boundary condition to obtain the steady-state condition. Then the boundary was changed to a stagnation inlet with an assigned value of pressure upstream of the inlet section, while preserving the value of flow rate obtained in the steady-state solution. The power was then increased in steps while searching for instability at each step. The problem with this method is that a constant pressure drop is imposed at the inlet of the channel for different powers, without considering the fact that changing the power changes the pressure drop as well.

In a very recent study, Xi et al. [6] carried out a 3-D numerical simulation of two heated parallel channels with supercritical water using CFX4, to find the instability boundaries. They used the geometry of Xiong et al. [8] and compared their results of instability thresholds with the experimental results of Xiong et al. [7]. They concluded that their 3-D model is capable of predicting the onset of instability in better agreement with the experiment than the 1-D code developed by Xiong et al. [8]. However, in their simulations, the number of nodes was relatively small considering their geometry. Also, they used special coupling methods for pressure and velocity, which are required when the code has an uncoupled solver, which was employed in their older version of CFX. The newer version of CFX (i.e. CFX5) is a fully coupled solver and therefore, the pressure-velocity coupling is inherent in the solution of the mass and momentum equation set. In addition, to find the instability boundary, they kept the total inlet mass flow rate constant and monitored the outlet mass flow rate during time with the increase of heat flux. Therefore, a constant pressure drop was imposed at the channel for different heat fluxes, without taking into account the variation of pressure drop with the power change.

Stability analysis of supercritical flow with CFD has the potential to provide a more accurate prediction of instability than 1-D codes. However, performing stability analysis using CFD is time-consuming and costly. Therefore, one use of CFD could be to assess the performance of 1-D codes. In the present work the static instability threshold in an up-flow heated tube with supercritical water is determined with the commercial CFD code: ANSYS CFX v14.5, using the standard k- ε model with a scalable wall-function and the SST model. Results are then compared with 1-D non-linear codes [9]. Also, conditions for approximating the thresholds of static instability threshold based on steady-state results [10, 3] are assessed and discussed.

1. Numerical Modelling

1.1 Geometry

The geometry, as shown in Figure 1, consists of a single circular vertical pipe with a length of 4.2672 m and a diameter of 8.36 mm, with a uniform heat flux applied at the wall. It is the same geometry used in previous CFD instability studies [4]. A fluid subdomain with an extra length of 0.0328 m is added at the outlet of the pipe for introducing a local pressure drop coefficient (K factor). In this study, only up-flow is considered and there is no inlet or outlet plenum. The flow is assumed to be axisymmetric. Therefore, a one-degree segment is used as shown in Figure 2 (a). A typical computational mesh is shown in Figure 2 (b).

1.2 Governing Equations

The governing equations of mass, momentum, energy, can be found in [11]. The turbulence models used in this study are the standard k-ε model with a scalable wall-function and the k-ω based SST model. The equations regarding these models are explained thoroughly in [11].

1.3 Boundary Conditions

Fluid Wall

No-slip conditions with an applied uniform heat flux were prescribed on the pipe wall.

Subdomain Fluid Wall

No-slip adiabatic condition was employed on the subdomain wall.

Inlet

In all cases, a uniform temperature was specified at the pipe inlet.

Steady-State: For steady-state conditions, an inlet mass flow rate was specified. For all of the cases studied, a different range of flow rate was examined to find the mass flow rate in which instability occurred. Flow direction was set normal to the boundary and the corresponding inlet velocity was uniform across the inlet. Also, a medium turbulence intensity of 5% was specified at the inlet. For medium intensity of 5%, CFX defines a viscosity ratio (μ_t/μ) equal to 10.
Transient: For a time-varying analysis, the initial conditions were a converged steady-state solution. Also, a medium turbulence intensity of 5% was specified as an initial condition across all domains for the transient solution. In addition, the inlet boundary condition was changed to an inlet with an average pressure equal to the pressure obtained from the steady-state solution. The corresponding flow and the turbulence condition were considered fully developed at the inlet.

Outlet

In all cases, at the pipe exit, an outlet condition with a static pressure equal to a reference pressure of zero was specified.

Symmetry

The flow was assumed to be axisymmetric. Therefore, the solution domain was 1/360 of the pipe volume. Symmetric boundary conditions were placed on the faces at zero and 1 degrees.

Domain Interface

A domain interface was defined between the main domain and the subdomain. This interface satisfied the conservation of mass, momentum, turbulence, and heat transfer between the two domains. There was a one-to-one correspondence of the mesh at the domain interface.

K Factor

An additional source term was added to the momentum equation, which was responsible for the isotropic loss. This term allows introducing the desired pressure drop into the momentum equation by specifying a loss coefficient at the fluid subdomain which is equivalent to the local pressure drop coefficient (K factor) in 1-D codes.

1.4 Property Variation

In CFX, properties of water are chosen to be calculated based on Thermodynamic Properties of Water and Steam from IAPWS-IF97 [12]. The range of validity for this property package is for temperatures from 0^{o}C to 800 ^{o}C and for pressures up to 100 MPa. When defining the density or specific heat capacity using IAPWS, the CFX-Solver generates tables of properties. These tables include the range of temperature and pressure and the maximum points. The parameter of maximum points specifies the maximum number of points (values) for each table dimension. The default value of 100 is not always adequate. In this study, the value was increased to 1000 points to increase the accuracy.

1.5 Mesh Generation

The mesh was generated using ANSYS ICEM CFD v14.5 software. Through different tests performed for the number of nodes in the angular direction, it was concluded that results are very sensitive to the number of angular nodes and to obtain a uniform solution of properties, a very fine resolution of mesh has to be applied in the angular direction. To reduce the computational costs, only 1/360 of the pipe volume was created since the flow was axisymmetric. Therefore, the main domain created is a wedge-shaped domain with an angle of 1^{o}. The diagram of the wedge-shaped solution domain with the angle exaggerated for clarity is shown in Figure 2 (a). Figure 2 (b) shows a coarse grid with an angle of 15^{o} to illustrate the concept of the grid used in the simulations.

A non-uniform distribution of nodes was used to obtain refinement near the pipe wall and a uniform distribution of nodes was used in the axial direction. A dimensionless distance of the first node from the wall, y+, was examined to ensure that it was consistent with the requirements of the turbulence model used.

1.6 Numerical Solution Method

The governing equations were solved using ANSYS CFX v.14.5. CFX discretizes the spatial domain into finite control volumes and the governing equations are integrated over each control volume, such that each quantity (mass, momentum, energy, etc.) is conserved for each control volume. Mass conservation discretization is applied on the grid with pressure-velocity coupling based on the work of Rhie and Chow [13]. The high-resolution advection scheme based on the work of Barth and Jesperson [14] is used. In the present study, computations were done with double precision. Steady-state solutions were considered converged when the maximum normalized residual of each of the discretized equations was less than 1×10^{-5} and the domain imbalance of equations solved was less than 0.01 %. Since a lower value of y^+ was used for the SST turbulence model, the convergence of the SST model was more difficult than the *k-ε* model and needed a smaller time step. For transient analyses, time step sizes of 0.1 s and 0.01 s were used for the *k-ε* and the SST models, respectively, and 10 full calculations were performed during each time step.

1.7 Mesh Independence Study

Ten grids with different numbers of nodes in different sections were created to examine the number of axial nodes, radial nodes, angular nodes, and near-wall spacing and to determine a grid with acceptable numerical accuracy. The axial variation average angular of wall temperature and the static pressure drop along the tube length were compared between the grids. It was realized that using the SST model, the results of average angular wall temperature are sensitive to the y^+ of the grid due to the strong variation of near-wall thermo-physical properties at supercritical pressures. In this study, the maximum y^+ of 0.1 (obtained using the first near-wall spacing of 1.5×10^{-4} mm) was found sufficient for grid independency. Also angular number of nodes equal to 7 was acceptable.

The mesh-independence tests were also conducted using coarse, medium, and fine meshes of 89,750, 311,960, and 635,400 nodes, respectively (for 1/360 of the geometry). Table 1 shows the number of nodes in different sections of the grids.

Table 1 Grids used for mesh independence study

Grid	Number of Nodes			First Near-Wall Spacing (mm)
	Axial	Radial	Angular	
Coarse	250	50	7	1.5×10^{-4}
Medium	440	100	7	1.5×10^{-4}
Fine	600	150	7	1.5×10^{-4}

The axial variation of average angular wall temperature and the static pressure drop along the tube length were determined and compared between grids. The RMS and maximum percentage difference of static pressure drop between coarse and medium grids were 89.69 Pa and 0.29% respectively, while these values were 2.61 Pa and 0.02%, respectively, between medium and fine

grids. For wall temperature, the RMS and maximum percentage difference between coarse and medium grids were 34.59 Pa and 25.45% respectively, while these values were 0.79 Pa and 0.55%, respectively, between medium and fine grids. Therefore, the medium grid was considered suitable. Finally, since a very small value of y^+ was used in the simulations, to decrease the maximum aspect ratio of the grid and improve the convergence rate, 600 axial nodes were implemented in the final mesh. Therefore, the final grid used in the simulations had axial, radial, angular numbers of nodes of 600, 100, and 7, respectively, and the value of first near-wall spacing was 1.5×10^{-4} mm.

2. Results and Discussion

The threshold for instability was determined using ANSYS CFX v.14.5 as follows:

Starting from a relatively high mass flow rate, a steady-state analysis was obtained first to determine the pressure drop between inlet and outlet of the pipe. In this steady-state analysis, the static pressure was specified at the outlet and the mass flow rate was specified at the inlet. This pressure drop was then used to specify the inlet static pressure for a transient analysis. The stability of the flow was determined by monitoring the inlet and outlet mass flow rates during the transient analysis.

In the case of static instability, the mass flow rate moves away from its equilibrium position in an excursive manner without returning to the original state (i.e. the mass flow rate drifts from its steady-state value to a higher or a lower value). In this study, for a stable case, a small difference was observed between the mass flow rate predicted by a transient run and the mass flow rate in the initial conditions that was derived from a steady-state run. This difference is due to the solution of the steady equations versus the transient equations. For a typical static instability case that difference was on the order of 0.13% in the mass flow rate. To ensure that the change in mass flow in a static instability case was due to the instability and not the above-mentioned numerical solution difference, a criterion for a minimum change in mass flow was developed. In this study, criterion of 1% change in mass flow rate was used to declare static instability and the instability threshold was taken as the higher mass flow rate value that the system drifted to over time (at least 20 s is needed to clarify that the flow is stable or unstable).

Table 2 shows the specifications of the cases used to study the static instability.

Table 2 Flow conditions for the cases used in the simulations, leading to static instability

Case	Reference Pressure (MPa)	Power (kW)	Inlet Temperature (C)	Outlet K Factor
S1	25	100	50	20
S2	25	100	50	15
S3	25	100	100	20
S4	25	100	100	15

Figure 3 (a) shows the inlet mass flow rate time response predicted by the CFD code for an initial mass flow rate of 0.0575 kg/s, an inlet temperature of 50°C, a power of 100 kW, and an outlet K factor of 20 (Case S1). The change in mass flow rate is 1.2%, indicating an unstable system. Figure 3 (b) shows the CFD response when the initial mass flow rate was 0.058 kg/s. The change in mass flow rate is 0.65% indicating a stable system. Thus, the instability threshold predicted by the CFD code is between 0.0575 kg/s and 0.058 kg/s. The higher values of instability boundary ranges are reported in this study, to assure the safety of the system.

Table 3 summarizes the static instability threshold results for the cases shown in Table 2, using the *k-ε* and the SST turbulence models and 1-D code. Results of instability thresholds between the *k-ε* and the SST models are close and the largest difference, which appears in Case S4, is 7.38% and for the other cases the difference is small. The SST and the *k-ε* turbulence models give similar predictions of the bulk flow properties. The main region where their results deviate is near the wall, where the SST model uses a much greater resolution of the turbulent boundary layer.

Table 3 Static instability threshold mass flow rates predicted by CFD and 1-D codes

Case	Instability Threshold Mass Flow Rate (kg/s)			Difference of Instability Threshold (%)		
	k-ε model	SST model	1-D Code	SST and *k-ε* models	*k-ε* model and 1-D Code	SST model and 1-D Code
S1	0.0585	0.058	0.058	0.86	0.85	0
S2	0.053	0.0525	0.056	0.95	5.66	6.67
S3	0.0625	0.0615	0.063	1.6	0.8	2.44
S4	0.0565	0.061	0.061	7.38	7.96	0

A 1-D non-linear code, SPORTS [9] was used to determine the static instability boundary for the same initial flow conditions. While a CFD code with a chosen turbulence model calculates the wall shear automatically via the wall functions used in the momentum equations, a 1-D code must rely on an empirical friction-factor correlation to determine the frictional pressure drop. The SPORTS code uses the Blasius [15] friction-factor formula for isothermal flow which is as follows:

$$f = 0.184\,\mathrm{Re}^{-0.2} \qquad \text{for} \qquad 3000 \leq \mathrm{Re} \leq 10^6 \qquad (1)$$

According to Table 3, the maximum difference of CFD and 1-D instability threshold is for Case S4, using the *k-ε* model. One of the reasons for the difference between 1-D and CFD instability results is the difference in the pressure drop prediction between these two codes. Also the calculation of pressure drop when having a K factor is not the same between the 1-D and the

CFD codes, since 1-D code calculates the pressure drop based on the bulk values of velocity and density, while in CFX, the pressure drop is calculated based on local values of velocity and density and is then area-averaged [11].

Ledinegg [10] and Chatoorgoon [3] have proposed conditions which make it possible to find the approximate threshold of static instability without a need to perform transient analyses. Ledinegg suggested that instability in two-phase flow occurs when the slope of the channel pressure drop versus mass flow rate curve is negative and steeper than the loop supply pressure-drop versus flow rate curve, which corresponds to the minimum of channel static pressure drop Δp versus mass flow rate plot. However, whether this condition applies to the supercritical flow is examined in this study. Chatoorgoon suggested that the minimum of $\Delta(p+\rho u^2)$ versus mass flow rate plot lies close to the static instability boundary for conditions with inlet and outlet plena. It is noteworthy that in this study, his condition is tested without inlet and outlet plena (it is difficult to conceive a system without inlet/outlet plenum). The plots in Figure 4 are the channel $\Delta(p+\rho u^2)$and the channel $\Delta(p)$ versus mass flow rate for the CFD code, using the *k-ε* and the SST models and the 1-D code, for Case S1. Then, the instability boundary point of the *k-ε* and the SST models and 1-D code are inserted into the curves of Figure 4.

Figures 5 and 6 summarize the results of ratio of mass flow rate at the instability boundary to the mass flow rate at the conditions specified for static instability, for the CFD and 1-D codes. These figures show that these ratios are between 0.9 and 1.1 for most of the cases, indicating a good agreement.

3. Conclusions

A numerical study was conducted to model a 2-D axisymmetric pipe with upward flow of supercritical water, using RANS models in ANSYS CFX v14.5 code. According to this study, the results of instability thresholds between the *k-ε* and the SST models were close and the largest difference, that appeared in Case S4, was equal to 7.38%. The difference was due to the fact that the *k-ε* model doesn't resolve the turbulent boundary details near the wall. Also, approximating the flow instability threshold by the minimum of $\Delta(p+\rho u^2)$ versus mass flow rate curve and the minimum of $\Delta(p)$ versus mass flow rate curve held true for a CFD solution. Ledinegg's criteria, however, agreed better with the CFD results (when there are no inlet and outlet plena). It is not known how well Ledinegg's condition will perform when there are inlet and outlet plena. That will be the subject of further studies.

4. References

[1] U.S. DOE Nuclear Energy Research Advisory Committee and the Generation IV International Forum, "A Technology Roadmap for Generation IV Nuclear Energy Systems", GIF, 2002.

[2] J.A. Boure, A.E. Bergles, and L. S. Tong, "Review of Two-Phase Flow Instability", Nuclear Engineering and Design 25, 1973, pp.165-192.

[3] V. Chatoorgoon, ”Non-dimensional parameters for static instability in supercritical heated channels”, Int. J. of Heat and Mass Transfer 64, 2013, pp.145-154.

[4] E. Ampomah-Amoako and W. Ambrosini, “Developing a CFD methodology for the analysis of flow stability in heated channels with fluids at supercritical pressures”, Annuals of Nuclear Energy 54, 2013, pp.251-262.

[5] W. Ambrosini, P.Di Marco, and A. Susanek, “Prediction of boiling channel stability by a finite-difference numerical method”, 2nd International Symposium on Two-Phase Flow Modeling and Experimentation, Pisa, Italy, 1999.

[6] X. Xi, Z. Xiao, X. Yan, T. Xiong, and Y. Huang, “Numerical simulation of the flow instability between two heated parallel channels with supercritical water”, Annals of Nuclear Energy 64, 2014, pp.57-66.

[7] T. Xiong, , X. Yan, Z.J. Xiao, Y.L. Li, Y.P. Huang, and J.C. Yu, “Experimental study on flow instability in parallel channels with supercritical water”, Annals of Nuclear Energy 48, 2012, pp.60-67.

[8] T.Xiong, X.Yan, Sh.Huang, J.Yu, and Y.Huang, “Modeling and analysis of supercritical flow instability in parallel channels”, Int. J. Heat and Mass Transfer 57, 2013, pp.549–557.

[9] V. Chatoorgoon, “SPORTS - A simple non-linear thermalhydraulic stability code”, Nuclear Engineering and Design, Volume 93, Issue 1, 1986, pp. 51–67.

[10] M. Ledinegg, “Instability of flow during natural and forced convection”, Die Warme, 61 (8), 1938, pp.891-898.

[11] E. Ebrahimnia, “Numerical stability and heat transfer analyses of supercritical water flowing upward in vertical heated pipes”, M.Sc Thesis, University of Manitoba, 2014.

[12] W. Wagner, J. R Cooper, A. Dittmann, J. Kijima, H.J. Kretzschmar, A. Kruse, R. Mares, K. Oguchi, H. Sato, I. Stocker, O. Sifner, Y. Takaishi, I. Tanishita, J. Trubenbach, and Th. Willkommen, “The IAPWS industrial formulation 1997 for the thermodynamic properties of water and steam, Journal of Engineering for Gas Turbines and Power”, Transactions of the ASME, Vol. 122, 2000.

[13] C.M. Rhie and W.L. Chow, “Numerical study of the turbulent flow past an air foil with trailing edge separation”, AIAA Journal 21, 1983, pp.1525-1532.

[14] T.J. Barth and D.C. Jesperson, “The design and application of upwind schemes on unstructured meshes”, AIAA Paper 89-0366, 1989.

[15] Blasius, H., Mitt.Forsch.Geb.Ing.-Wesen 131, 1913, pp.1-41.

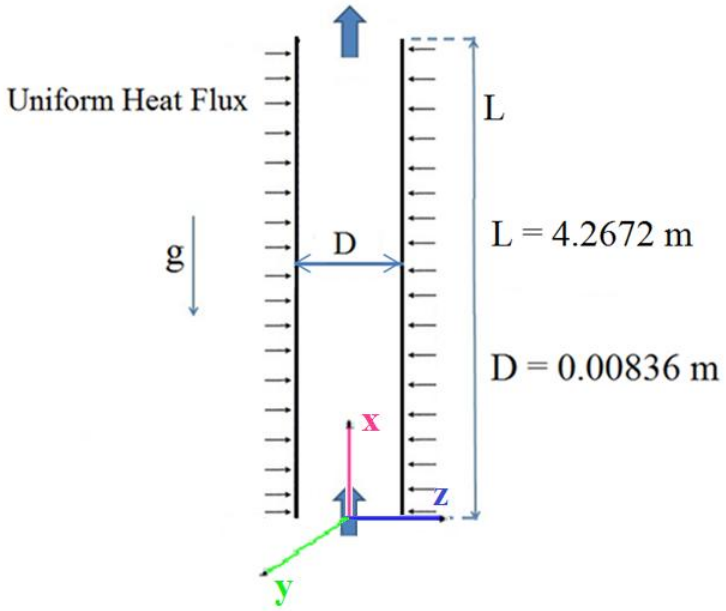

Figure 1 Geometry of the vertical pipe used for simulations

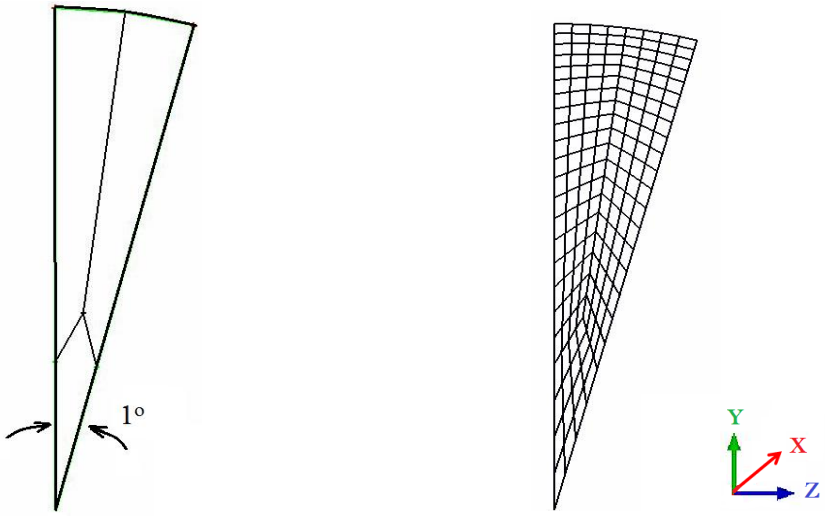

(a) (b)

Figure 2 A cross sectional view of the a) geometry blocking in ICEM CFD and b) typical coarse mesh (the angle is exaggerated for clarity)

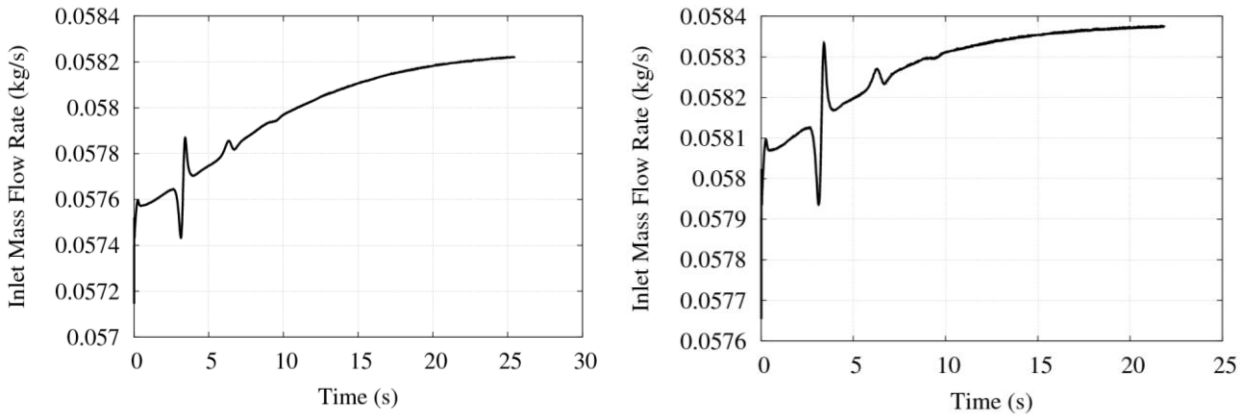

(a) (b)

Figure 3 CFD results for a) an unstable and b) a stable case using the SST model for Case S1

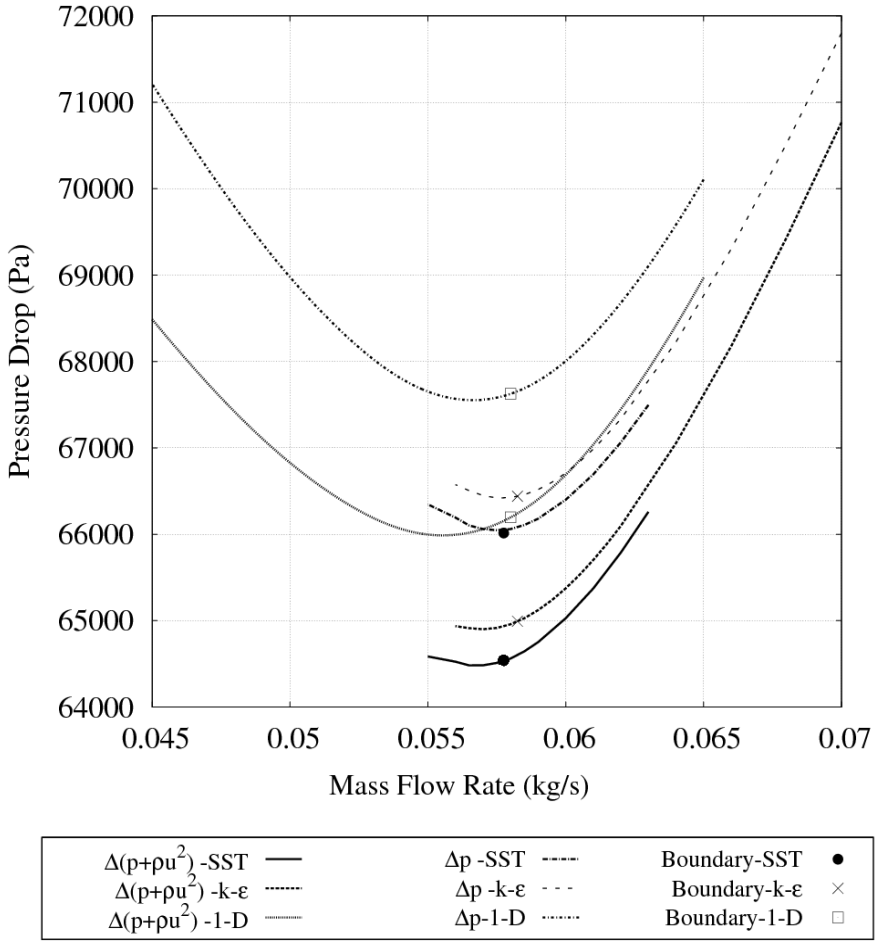

Figure 4 Instability boundary and $\Delta(p+\rho u^2)$ and Δp of the channel versus mass flow rate using the *k-ε* and the SST models and 1-D code for Case S1

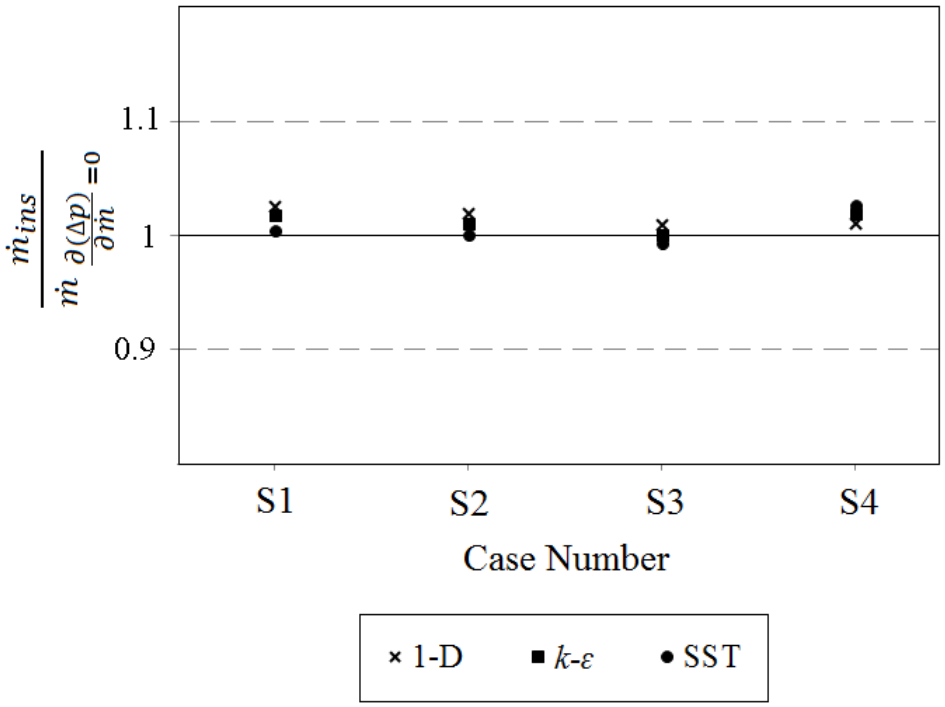

Figure 5 Ratio of mass flow rate at the instability boundary to the mass flow rate at $\partial\,(\Delta \mathrm{p})/\partial \dot{\mathrm{m}}$ = 0 for static instability cases using CFD and 1-D codes

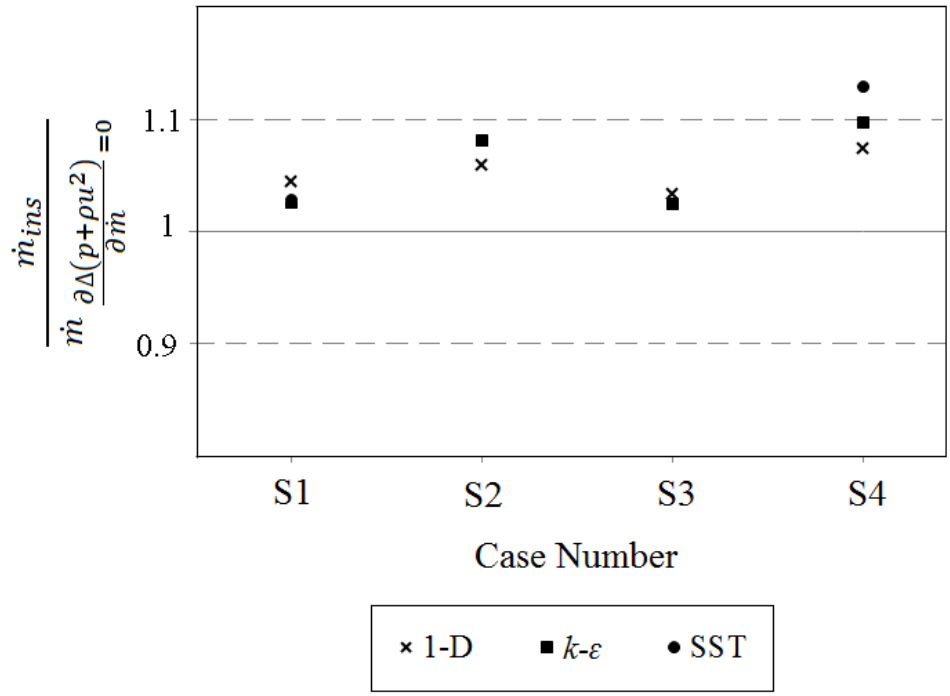

Figure 6 Ratio of mass flow rate at the instability boundary to the mass flow rate at $\partial\,\Delta(\mathrm{p}+\rho \mathrm{u}^2)/\partial \dot{\mathrm{m}}$ = 0 for static instability cases using CFD and 1-D codes